

EFFECTS OF FRICTION AND CUTTING SPEED ON CUTTING FORCE

Troy D. Marusich
Third Wave Systems, Inc
Minneapolis, MN

ABSTRACT

Observations are made regarding the influence of cutting speed and friction on cutting force by way of finite element modeling. Simulations are validated by comparison of cutting forces and chip morphologies for the Al6061-T6. Analysis of cutting forces over a wide range of cutting conditions suggests an important role of the secondary shear zone in the decrease of cutting force as a function of speed, even well into what is considered to be the adiabatic machining regime. The proposition is supported by a decrease in chip thickness and significant increase in temperature at the tool-chip interface as the speed is increased. Temperatures in the primary shear zone rise only modestly and cannot account for the change in cutting force. Furthermore, the effect contributes to the nonlinear increase of forces with respect to feed as opposed to a plowing force by the cutting edge radius.

INTRODUCTION

In order to improve metal cutting processes, i.e. lower part cost, it is necessary to model metal cutting processes at a system level. A necessary requirement of such is the ability to model interactions at the tool chip interface and thus, predict cutter performance. Many approaches such as empirical, mechanistic, analytical and numerical have been proposed. Some level of testing for model development, either material, machining, or both is required for all. However, the ability to model cutting tool performance with a minimum amount of testing is of great value, reducing costly process and tooling iterations. In this paper, a validated finite element-based machining model is presented and employed to determine the effects of friction and workpiece strength in the secondary shear zone on cutting forces.

Typical approaches for numerical modeling of metal cutting are Lagrangian and Eulerian techniques. Lagrangian techniques, the tracking of discrete material points, has been applied to metal cutting for over a decade (Strenkowski and Carroll, 1985; Komvopoulos and Erpenbeck, 1991; Sehkou and Chenot, 1993; Obikawa and Usui, 1996; and Obikawa *et. al* 1997.). Techniques typically used a predetermined line of separation at the tool tip, propagating a fictitious crack ahead of the tool. This method precludes the resolution of the cutting edge radius and accurate resolution of the secondary shear zone due to severe mesh distortion. To alleviate element distortions, others used adaptive remeshing techniques to resolve the cutting edge radius (Sehkou and Chenot, 1993; and Marusich and Ortiz, 1995). Eulerian approaches, tracking volumes rather than material particles, did not have the burden of rezoning distorted meshes (Strenkowski and Athavale, 1997). However, steady state free-surface tracking algorithms were necessary and relied on assumptions such as uniform chip thickness, precluding the modeling of milling processes or segmented chip formation .

In this paper, a Lagrangian finite element-based machining model is applied to orthogonal cutting of Al6061-T6. Techniques such as adaptive remeshing, explicit dynamics and tightly couple transient thermal analysis are integrated to model the complex interactions of a cutting tool and workpiece.

MACHINING SIMULATION SYSTEM

Simulations were performed with Third Wave Systems *AdvantEdge* machining simulation software, which integrates specialized finite element numerics and material modeling appropriate for machining. The orthogonal cutting system is described in Fig. 1 where the observer is in the frame of reference of the cutting tool with the workpiece moving with velocity v . The cutting tool is parameterized by rake and

clearance angles, and a cutting edge radius. In the plane strain case the depth of cut into the plane is considered to be large in comparison to the feed. The cutting tool initially indents the workpiece, Fig. 2, the chip begins to form Fig. 3, and finally curls over hitting the workpiece ahead of the cut, Fig. 4.

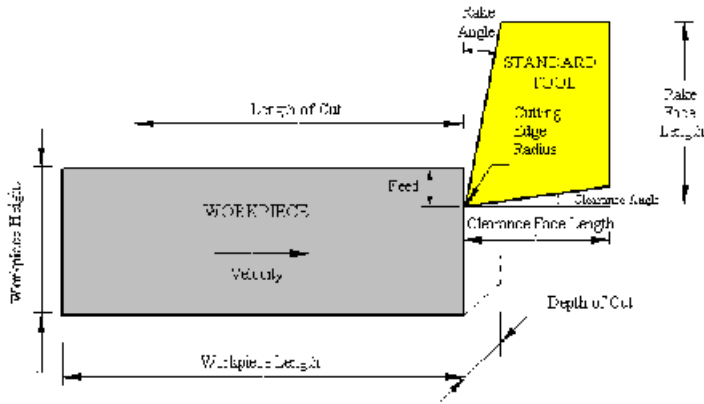


Figure 1 Schematic of orthogonal cutting conditions.

Integration by parts and rearranging terms provides

$$\int_B \rho v_i \ddot{u}_i dV + \int_B v_{i,j} \sigma_{ij} dV = \int_{\partial B} v_i \sigma_{ij} n_j d\Omega + \int_B v_i \rho b_i dV$$

which can be interpreted as

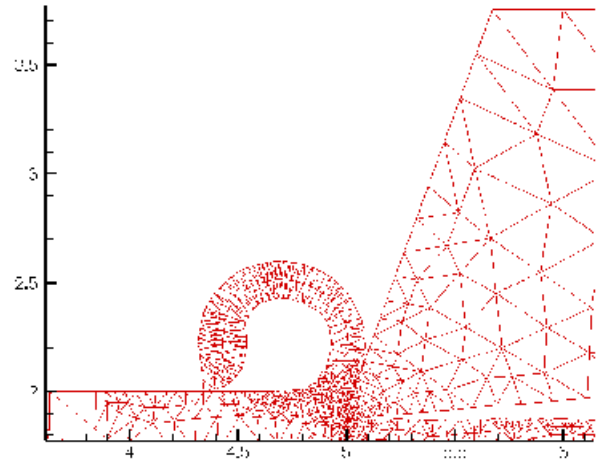


Figure 3 Chip formation

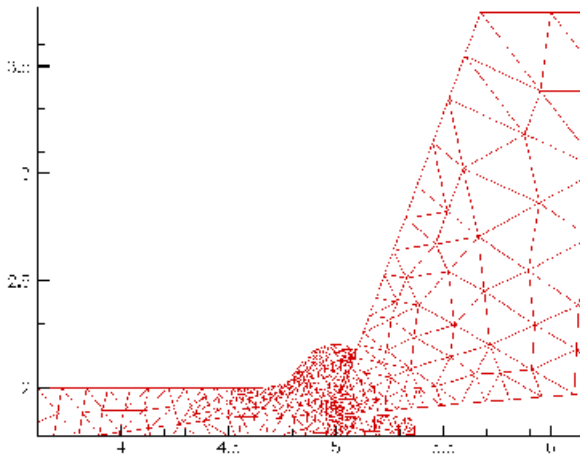


Figure 2 Initial tool indentation

The balance of linear momentum is written as

$$\sigma_{ij,j} + \rho b_i = \rho \ddot{u}_i$$

The weak form of the principle of virtual work becomes

$$\int_B v_i \sigma_{ij,j} + v_i \rho b_i dV = \int_B \rho v_i \ddot{u}_i dV$$

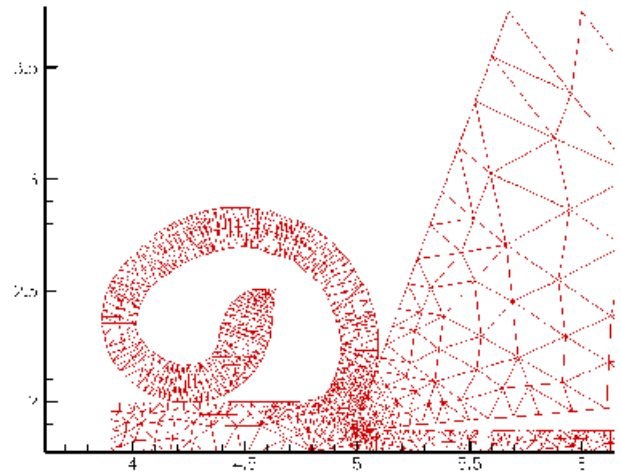


Figure 4 Fully developed continuous chip

(Inertial Terms) + (Internal Forces) = (External Forces) + (Body Forces)

Finite element discretization provides

$$\int_B \rho N_a N_b \ddot{u}_{ib} dV + \int_B N_{a,j} \sigma_{ij} dV = \int_{\partial B} N_a \tau_i d\Omega + \int_B \rho N_a b_i dV$$

In matrix form

$$\mathbf{M} \mathbf{a}_{n+1} + \mathbf{R}_{n+1}^{\text{int}} = \mathbf{R}_{n+1}^{\text{ext}}$$

where

$$M_{ab} = \int_{B0} \rho_0 N_a N_b dV_o$$

is the mass matrix

$$R_{ia}^{\text{ext}} = \int_{B0} b_i N_a dV_o + \int_{\partial B0} \tau_i N_a d\Omega_o$$

is the external force array and

$$R_{ia}^{\text{int}} = \int_{B0} P_{ij} N_{a,j} dV_o$$

is the internal force array. In the above expressions, $N_{a=1, \dots, \text{numnp}}$ are the shape functions, repeated indices imply summation, and a comma (,) represents partial differentiation with respect to the corresponding spatial coordinate, and P_{ij} is the first Piola-Kirchhoff stress tensor, analogous to the engineering or nominal stress.

Thermal Equations

Heat generation and transfer are handled via the second law of thermodynamics. A discretized weak form of the first law is given by

$$\mathbf{C}\dot{\mathbf{T}}_{n+1} + \mathbf{K}\mathbf{T}_{n+1} = \mathbf{Q}_{n+1}$$

A lumped capacitance matrix \mathbf{C} is used to eliminate the need for any equation solving.

$$\mathbf{C}\dot{\mathbf{T}} + \mathbf{K}\mathbf{T} = \mathbf{Q}$$

where \mathbf{T} is the array of nodal temperatures,

$$C_{ab} = \int_{Bt} c\rho N_a N_b dV_o$$

is the heat capacity matrix,

$$K_{ab} = \int_{B0} D_{ij} N_{a,i} N_{b,j} dV$$

is the conductivity matrix, and

$$Q_a = \int_{Bt} s N_a dV + \int_{B\tau q} h N_a dS$$

is the heat source array with h , having the appropriate value for the chip or tool.

In machining applications, the main sources of heat are plastic deformation in the bulk and frictional sliding at the tool-

workpiece interface. The rate of heat supply due to the first is estimated as

$$s = \beta \dot{W}^p$$

where \dot{W}^p is the plastic power per unit deformed volume and the Taylor-Quinney coefficient β is of the order of 0.9. The rate at which heat is generated at the frictional contact, on the other hand is

$$h = -\mathbf{t} \cdot \llbracket \mathbf{v} \rrbracket$$

where \mathbf{t} is the contact traction and $\llbracket \mathbf{v} \rrbracket$ is the jump in velocity across the contact.

Modeling Approach

AdvangEdge is an explicit dynamic, thermo-mechanically coupled finite element model specialized for metal cutting. Features necessary to model metal cutting accurately include adaptive remeshing capabilities for resolution of multiple length scales such as cutting edge radius, secondary shear zone and chip load; multiple body deformable contact for tool-workpiece interaction, and transient thermal analysis.

A major thrust of this paper is the investigation of the effect of friction at the tool-chip interface which is dominated by heating of the secondary shear zone. The characteristic length scale (CLS) involved is typically one order of magnitude smaller than the chip load in common turning and milling operations. In order to resolve the secondary shear zone CLS and the inherent large deformations while maintaining computationally accurate finite element configurations, adaptive remeshing techniques are critical and employed within the present analysis. Near the cutting edge radius, the workpiece material is allowed to flow around the edge radius. The initial mesh, Fig. 5, becomes distorted after a certain length of cut, Fig. 6, and is remeshed in this vicinity to form a regular mesh again, Fig. 7. For a comprehensive discussion on the numerical techniques the reader is referred to Marusich and Ortiz (1995).

Constitutive Model and Material Characterization

In order to model chip formation, constitutive modeling for metal cutting requires determination of material properties at high strain rates, large strains, and short heating times and is quintessential for prediction of segmented chips due to shear-localization (Sandstrom and Hodowany 1998; Childs, 1998). Specific details of the constitutive model used are outlined in Marusich and Ortiz (1995). The model contains deformation hardening, thermal softening and rate sensitivity tightly coupled with a transient heat conduction analysis appropriate for finite deformations.

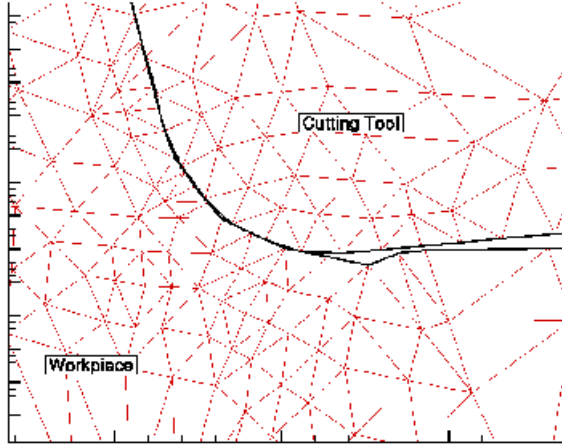


Figure 5 Initial mesh around tool and workpiece

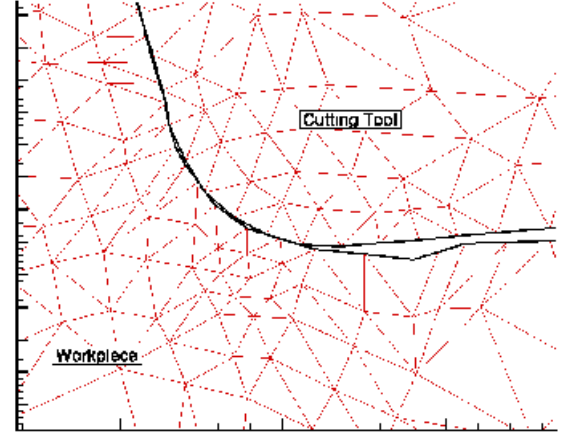


Figure 7 Updated workpiece mesh

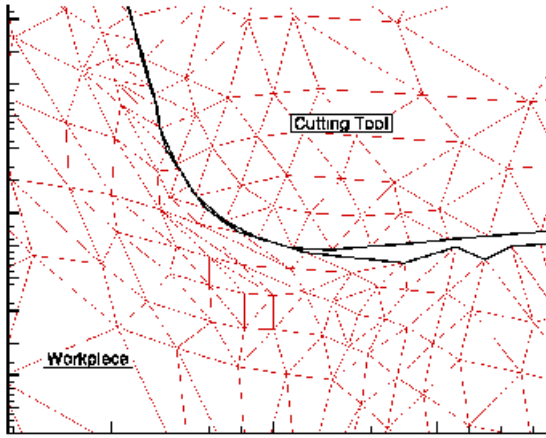


Figure 6 Deformed workpiece mesh

There is substantial material test information available for Al6061-T6 in terms of deformation hardening, thermal softening and high strain rate response. Typical properties found in the open literature were used for model development (e.g., initial yield stress and deformation hardening, thermal softening). The friction coefficient for the stick-slip Coulomb model is calibrated from cutting test data and is best determined at low cutting speeds where effects of the secondary shear zone become less dominant. The friction coefficient is the only such model parameter that relies on cutting test data and is held constant for the subsequent analyses.

In a typical high-speed machining event, very high strain rates in excess of 10^5 s^{-1} may be attained within the primary and secondary shear zones. The increase in flow stress due to strain rate sensitivity is accounted for with the relation

$$\left(1 + \frac{\dot{\epsilon}^p}{\epsilon_0^p}\right) = \left(\frac{\bar{\sigma}}{g(\epsilon^p)}\right)^{m_1}$$

where $\bar{\sigma}$ is the effective Mises stress, g the flow stress, ϵ^p the accumulated plastic strain, ϵ_0^p a reference plastic strain rate, and m_1 is the strain rate sensitivity exponent

A power hardening law model is adopted with thermal softening. This gives

$$g = \sigma_0 T(T) \left(1 + \frac{\epsilon^p}{\epsilon_0^p}\right)^{1/n}$$

where n is the hardening exponent, T the current temperature, and σ_0 is the initial yield stress at the reference temperature T_0 , ϵ_0^p the reference plastic strain, and $T(T)$ is a thermal softening factor ranging from 1 at room temperature to 0 at melt and having the appropriate variation in between.

To characterize the Al6061-T6 workpiece material, test data from published literature was used. Constitutive model parameter values for the mechanical and heat transfer responses

are shown in Table 1. Quasi-static tension test data at room temperatures (ASM, 1974) was used to determine strain hardening values while elevated temperature test data was used to determine thermal softening coefficients (ASM, 1974). Parameter values for strain rate sensitivity were determined by comparing elevations in flow stress across a range of strain rates (Maiden and Green, 1966; Nicholas, 1981) from near quasi-static (e.g., 0.01/s) to high rate ($\sim 10^3$ - 10^4 /sec)

Table 1 Mechanical and thermal material constants

Material Constant	Value	Units
σ_0	282	MPa
p	4.26	10^{-3}
e_0		
n	12.35	
m_1	140	
$\dot{\epsilon}_0^p$	10	sec^{-1}
μ	0.2	
E	69	GPa
ν	0.33	
ρ	2700	kg/m^3
c	921	J/kgC
k	180	W/mC

Table 2 Cutting conditions for Al6061-T6 validation

Case	Rake Angle	Feed mm/rev	Speed m/min
1	20^0	0.2489	631
2	40^0	0.2489	175
3	20^0	0.1245	631
4	40^0	0.0506	175
5	40^0	0.1242	175
6	40^0	0.1867	175

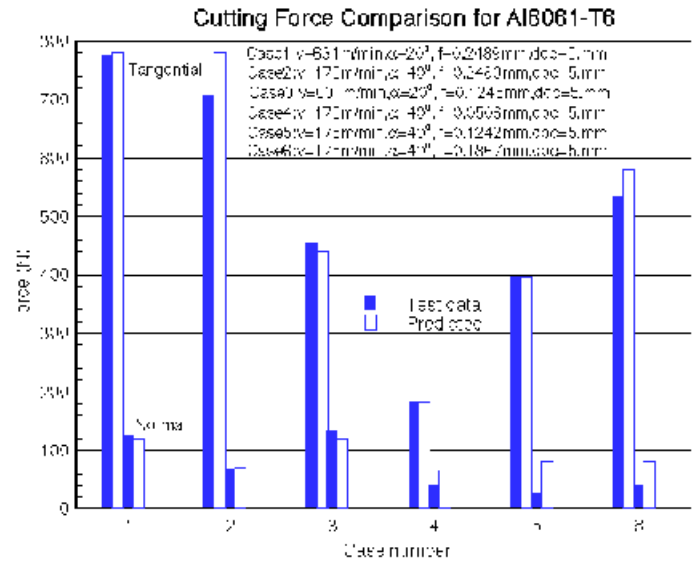


Figure 8 Comparison between predicted and measured cutting force components over a range of cutting conditions.

SIMULATION VALIDATION

The primary metrics for validating the simulation system are cutting forces and chip thickness. Comparison over a wide range of industrially accepted cutting conditions provides validation of the numerical-constitutive integration response. Once the simulation system has been validated further analysis may be performed over a wider range of conditions, taking advantage of the first principals approach.

Cutting Force Comparison

Cutting force components tangential and normal to the cutting direction were compared for those generated during orthogonal tube turning in the case of Al6061-T6. Cutting conditions for Al6061-T6 are shown in Table 2 (Kobayashi *et al.*, 1960). All simulations were performed with an edge radius of 0.015mm as to minimize the introduction of an additional length scale at low feeds.

The predicted and measured cutting forces are compared for Al6061-T6 in Fig. 8. The cutting conditions vary over a sufficiently large parameter space and establish confidence in the model results. Cutting forces generally agree within 10% of the measured values for both tangential and normal components, as well as the corresponding trends with changes in cutting conditions.

Chip Morphology

Kobayashi *et al.* (1960) observed continuous chip morphologies for the conditions investigated, i.e., segmentation due to adiabatic shear banding or local fracture was not observed. Additionally, no mention of built up edge was made. Consequently, predicted and measured chip thickness comparisons can be made readily, Fig. 9. Once again good agreement is made over the range of cutting conditions where the simulations retain the corresponding trends with variation in cutting. The finite element model typically over predicts the cutting forces due to plane strain assumptions made, with numerical convergence of the mesh approaching from the “stiff” side of the solution. Once the material models have been validated, extrapolation to new cutting conditions (e.g., speed, cutter geometry) can be made with confidence due to the first-principles approach.

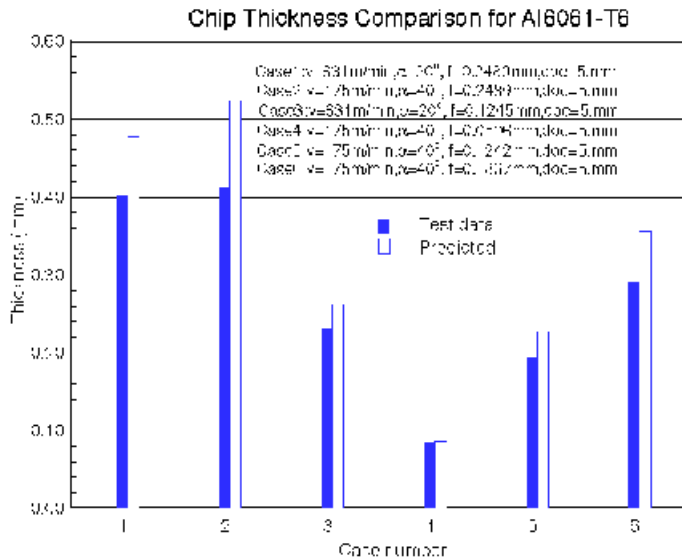


Figure 9 Comparison between predicted and measured chip thickness over a range of cutting conditions.

RESULTS

Cutting Speed Effects

To determine the mechanisms for the reduction in cutting force with increase in speed, simulations were performed at very low speeds and progressively increased to high speed machining regimes, Table 3. The speed range was covered for feeds of 0.25mm/rev and 0.075mm/rev. A significant reduction in cutting force is observed as the cutting speed increases, Fig. 10, particularly at high chip loads. This is a well-documented phenomenon for a number of materials (Flom, 1983; and Smart and Trent, 1975). Smaller decreases as a percentage are seen at lighter chip loads, Fig. 10. Similar trends are seen for chip thickness, as it decreases with increasing cutting speed Fig. 11. Again, the most prominent relative changes occurring at higher chip loads. Specific cutting forces computed from the normalization of force with chip load are shown in Fig. 12. It is seen that specific cutting forces for low chip loads are higher, i.e. material removal is more energetically expensive at light chip loads.

Temperature profiles in the primary shear zone increase slightly for both chip loads, Fig. 13. However, the secondary shear zone temperature increases substantially for both chip loads, with maximum temperature for the highest chip load, Fig. 13.

For both chip loads the shear angle increases, indicating a reduction in apparent friction with increasing speed, Fig. 14. However, the most dramatic change in shear angle over the speed range is seen at high chip loads. Interfacial shear stress reduces with increasing temperature, Fig. 15, the end result of a softening material in the secondary shear zone at higher strain rates, Fig. 16.

Chip Load Effects

Simulations were performed at constant cutting speed of 600m/min over a range of chip loads, Table 3. Cutting forces were seen to increase with chip load, Fig. 17. However, when normalized cutting forces are plotted the result is a reduction at high chip loads, i.e., the cutting process becomes more efficient at higher chip loads. The resulting linear extrapolation of cutting forces at moderate and high chip loads to zero chip load does not yield zero cutting force (Stevenson and Stephenson, 1995). Consequently, the mechanics of the cutting process are influenced by the chip load.

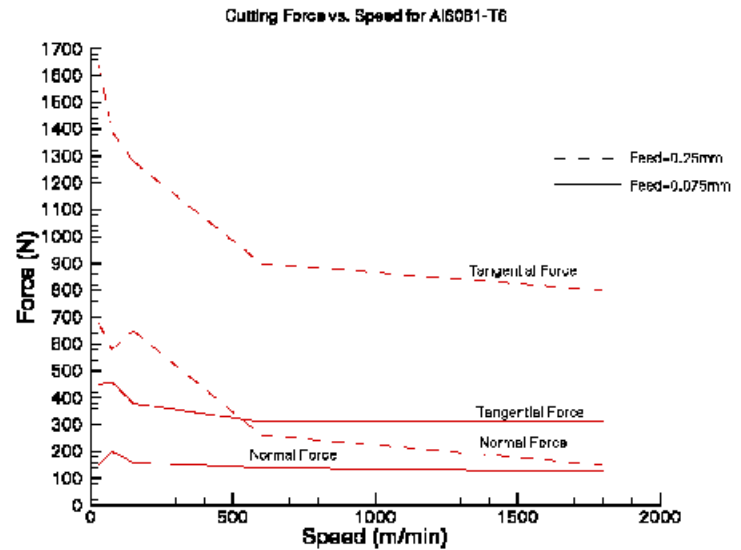


Figure 10 Cutting force components vs. speed at 0.25mm and 0.075mm feed.

Table 3 Simulation conditions for Al6061-T6

Case	Rake Angle	Feed mm/rev	Speed m/min
1	10^0	0.250	60
2	10^0	0.250	120
3	10^0	0.250	250
4	10^0	0.250	600
5	10^0	0.250	1800
6	10^0	0.075	60
7	10^0	0.075	120
8	10^0	0.075	250
9	10^0	0.075	600
10	10^0	0.075	1800
11	10^0	0.050	600
12	10^0	0.150	600
13	10^0	0.350	600

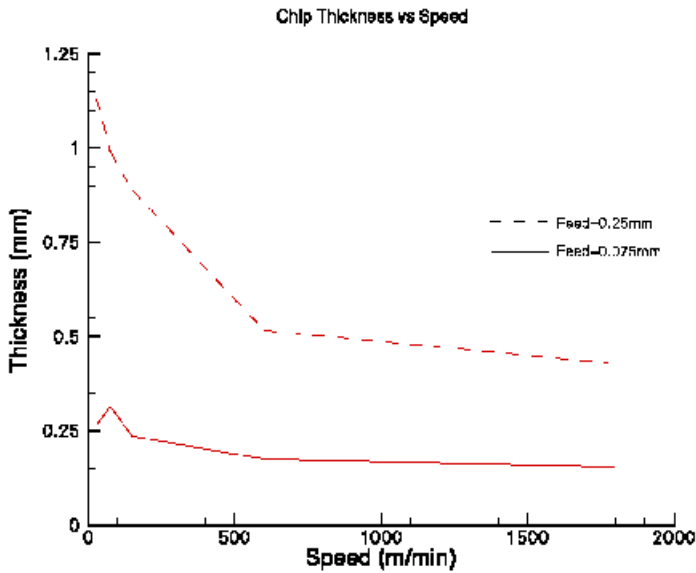


Figure 11 Chip thickness vs. speed for feeds of 0.25mm and 0.075mm

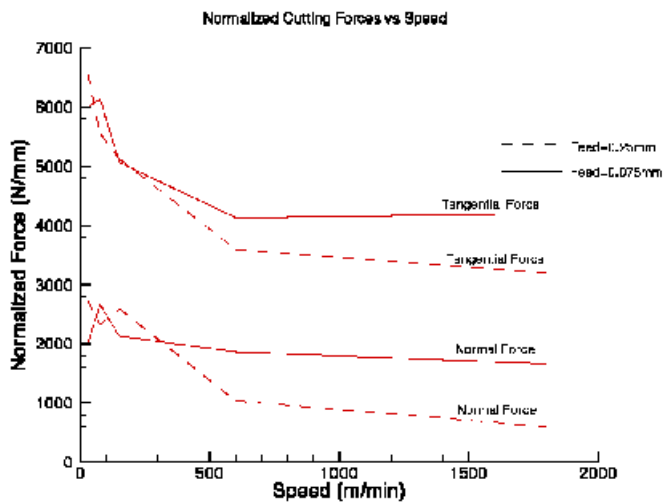


Figure 12 Normalized cutting forces for feeds of 0.25mm and 0.075mm.

DISCUSSION

Cutting Speed Effects

The decrease in cutting forces with increase in cutting speed is well documented in literature. However, the mechanism for such an effect has not been readily accepted to date. The finite element simulations reproduce the correct trends and magnitudes of cutting force with speed for different

chip loads, Figs. 8,10. The increase in temperature of the primary shear zone is less than 100°C at the highest chip load and peaks around 200 °C, Fig. 13. The corresponding decrease in flow stress in the primary shear zone due to thermal softening effects can not account for a near 50% reduction in cutting force, Fig. 10. In addition, isolating the thermal softening effects does not take into account any competing effects in the flow stress by the strain rate hardening at higher speeds, Fig. 16. The decrease in cutting force must come from the reduction in effective friction at the tool-chip interface. A reduction in apparent friction at the tool-chip interface is evidenced by the thinning of the chip at higher cutting speeds

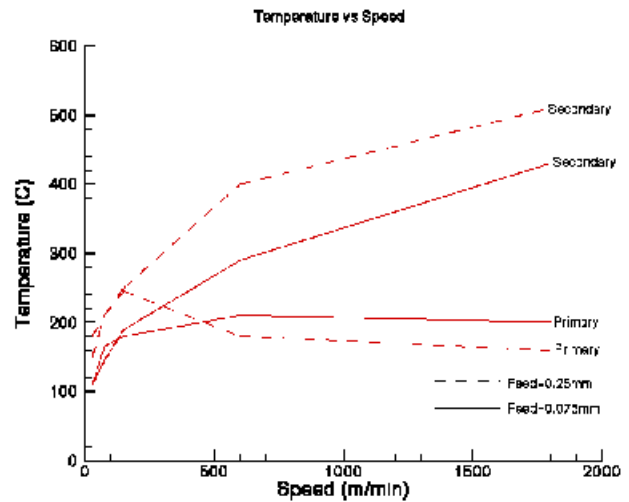


Figure 13 Temperature in primary and secondary shear zones vs. speed

As previously mentioned the increase in temperature in the primary shear zone will not result in a substantial decrease in flow stress however, the secondary shear zone temperatures rise nearly 400°C, Fig. 13., allowing for significant reduction in flow stress, Fig. 15. Additionally, the chip thickness decreases with increasing cutting speed, Fig. 11., accompanied by the corresponding increase in shear plane angle, Fig. 14., indicating the relative reduction in flow stress between primary and secondary shear zones is greatest at the tool chip interface. Again, this is seen as a reduction in the apparent coefficient of friction. The end result is more efficient chip formation at higher cutting speeds and chip loads as seen through a reduction in normalized cutting force, Fig. 12. While normalized cutting forces are approximately the same at low cutting speeds for both chip loads, substantial decreases in normalized cutting force occurs for larger chip loads at higher speeds.

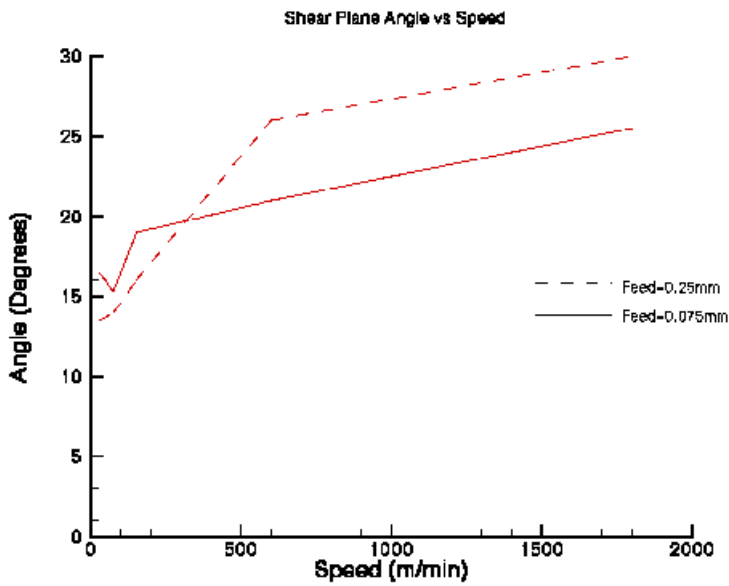


Figure 14 Primary shear plane angle as a function of speed and feed.

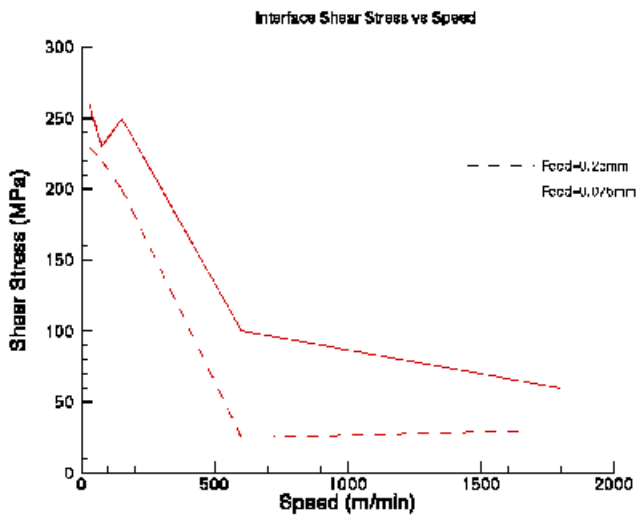


Figure 15 Shear stress at the tool-chip interface as a function of speed and feed.

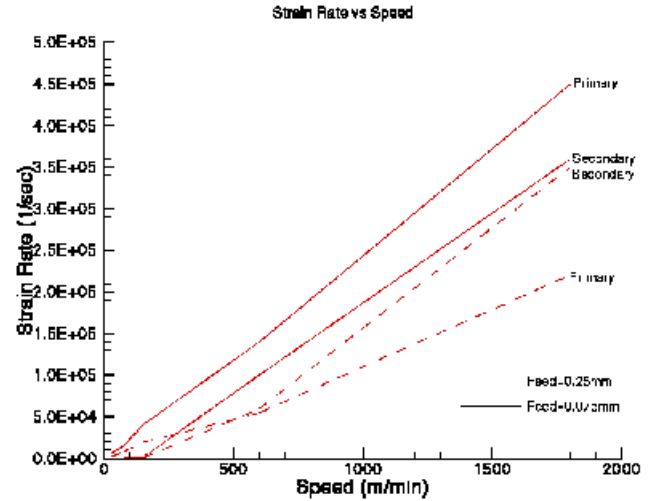


Figure 16 Strain rate in primary and secondary shear zones as a function of speed and feed.

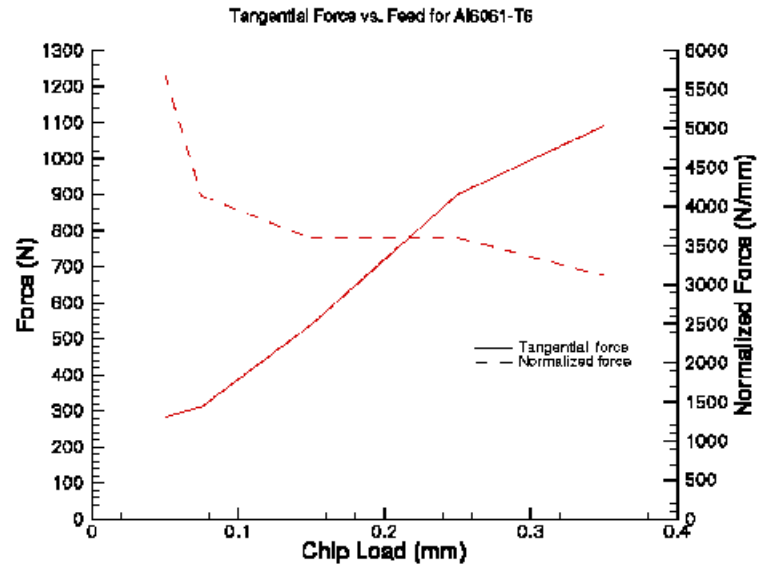


Figure 17 Tangential force and normalized force vs. chip load at $v=600\text{m/min}$.

Chip Load Effects

Specific cutting forces are highest for lower chip loads, Fig. 12. Normalized cutting forces are seen to increase as the chip load is decreased for a constant cutting speed evidently, the most efficient cutting is at high cutting speeds and chip loads. Extrapolating the cutting force to zero chip load in Figure 12. results in a non-zero cutting force, studied extensively by Stevenson and Stephenson (1995). In order for

the cutting to become efficient it is necessary for the secondary shear zone to become fully developed at the tool-chip interface. The width of the primary and secondary shear zones provide the CLS in the continuum analysis and will predominantly be set by material properties such as rate sensitivity, work hardening and thermal softening. For the secondary shear zone to become fully developed it must be the length of a number of CLS along the tool-chip interface. If this is not the case, the material is not fully softened and a higher apparent friction is realized. The proposition is supported by the normalized cutting forces flattening out at higher chip loads, Fig 17.

The overall governing effect of friction is actually the material flow strength in the secondary shear zone at the tool-chip interface at higher speeds. At lower chip loads the secondary shear zone can not fully develop, thus the full reduction in interfacial strength is not realized. At higher chip loads a sufficient number of CLS exists along the tool-chip interface to afford full reduction in interfacial strength and consequently, cutting force.

CONCLUSION

Finite element simulations are validated by comparison of cutting forces and chip morphologies for the Al6061-T6. Analysis of cutting forces over a wide range of cutting conditions suggests an important role of the secondary shear zone in the decrease of cutting force as a function of speed, even well into regimes where primary shear zone temperatures have stabilized. The proposition is supported by a decrease in chip thickness and significant increase in temperature at the tool-chip interface as the speed is increased, while the temperatures in the primary shear zone rise only modestly and cannot account for the change in cutting force. Furthermore, the effect contributes to the nonlinear increase of forces with respect to feed and not due to a plowing effect of the cutting edge radius.

REFERENCES

"Aerospace Structural Metals Handbook", ASM International, **2** (1974), 29-51.

Childs, T. H. C., "Material Property Needs in Modelling Metal Machining," *CIRP Workshop on Modeling Metal Cutting*, (1998).

Flom, D. G., "High-Speed Machining," in: Bruggeman and Weiss (eds.) *Innovations in Materials Processing*, Plenum Press, (1983), 417-439.

Kobayashi, S., Herzog, R. P., Eggleston, D. M. and Thomsen, E. G., "A Critical Comparison of Metal-Cutting Theories with New Experimental Data", *Trans. ASME J. Eng. Ind.* (1960), 333-347.

Komvopoulos, K. and Erpenbeck, S.A., "Finite Element Modeling of Orthogonal Metal Cutting," *J. Engrg. Ind.*, **113** (1991), 253-267.

Maiden, C. J. and Green, S. J., "Compressive Strain-Rate Tests on Six Selected Materials at Strain Rates from 10^{-3} to 10^4 /sec," *Trans. ASME J. Appl. Mech.* (1966), 496-504.

Marusich, T. D. and Ortiz, M., "Modeling and Simulation of High-Speed Machining", *Int. J. Num. Meth. Eng* **38** (1995), 3675-94.

Nicholas, T., "Tensile Testing of Materials at High Rates of Strain", *Experimental Mechanics*, (1981), 177-185.

Sandstrom, D. R. and Hodowany, J. N., "Modeling the Physics of Metal Cutting in High-Speed Machining," *Machining Science and Technology*, **2** (1998), 343-353.

Sekhon, G.S. and Chenot, J.L., "Numerical Simulation of Continuous Chip Formation During Non-Steady Orthogonal Cutting," *Engineering Computations*, **10** (1993), 31-48.

Smart, E. F. and Trent, E. M., "Temperature Distributions in Tools Used for Cutting Iron, Titanium and Nickel," *Int. J. Prod. Res.*, **13** (1975), 265-290.

Stevenson, R. and Stephenson, D. A., "The Mechanical Behavior of Zinc During Machining," *Journal of Engineering Materials and Technology*, **177** (1995), 172-178.

Strenkowski, J. S. and Athavale, S. M., "A Partially Constrained Eulerian Orthogonal Cutting Model for Chip Control Tools," *Journal of Manufacturing Science*, **119** (1997), 681-688.

Strenkowski, J. S. and Carroll, J.T., III, "A Finite Element Model of Orthogonal Metal Cutting," *J. Engrg. Ind.*, **107** (1985), 349-354.

Obikawa, T. and Usui, E., "Computational Machining of Titanium Alloy-Finite Element Modeling and a Few Results," *Journal of Manufacturing Science and Engineering*, **118** (1996).

Obikawa, T., Sasahara, H., Shirakashi, T. and Usui, E., "Application of Computational Machining Method to Discontinuous Chip Formation," *Journal of Manufacturing Science and Engineering*, **119** (1997), 667-674.

